

Microscopic Theory of Γ_3 Quadrupole Ordering in Pr Compounds on the Basis of a j - j Coupling Scheme

Ryosuke Yamamura and Takashi Hotta

Department of Physics, Tokyo Metropolitan University, Hachioji, Tokyo 192-0397, Japan

(Received February 18, 2019)

Toward the understanding of incommensurate Γ_3 quadrupole ordering in PrPb₃, we develop a microscopic theory of multipole ordering in f^2 -electron systems from an itinerant picture on the basis of a j - j coupling scheme. For this purpose, we introduce the Γ_7 - Γ_8 Hubbard model on a simple cubic lattice with the effective interactions that induce local Γ_3 states. By evaluating multipole susceptibility in a random phase approximation, we find that the hybridization between Γ_7 and Γ_8 orbitals plays a key role in the emergence of Γ_3 quadrupole ordering. We also emphasize that Γ_3 quadrupole ordering can be understood from the concept of *multipole nesting*, in which the Fermi surface region with large Γ_8 orbital density should be nested on the area with a significant Γ_7 component when the positions of the Fermi surfaces are shifted by the ordering vector. This concept can be intuitively understood from the fact that local Γ_3 doublets are mainly composed of two singlets between Γ_8 and Γ_7 orbitals. Finally, we discuss the possible relevance of the present theory to the experimental results of PrPb₃ and point out some future problems in this direction of research.

1. Introduction

In recent decades, multipole ordering in f -electron systems has attracted continuous attention in the research field of condensed matter physics.¹⁻⁴⁾ In general, a multipole is considered to be a spin-orbital complex degree of freedom emerging in a system in which spin and orbital degrees of freedom are tightly coupled with each other due to a strong spin-orbit interaction. A description of multipole degrees of freedom has been provided on the basis of the Stevens' operator-equivalent technique.⁵⁾ Among the f -electron systems, rare-earth and actinide compounds with multiple f electrons per ion exhibit diverse multipole phenomena. In particular, for the case of $n = 2$, where n denotes the local f -electron number, intriguing phenomena originating from non-Kramers degeneracy have been discussed for a long time. A typical example is considered to be the two-channel Kondo effect, which is expected to occur in U and Pr ions with the Γ_3 ground state.^{6,7)} Another example is the modulated antiferro Γ_3 O_2^0 quadrupole ordering observed in PrPb₃ with the AuCu₃-type simple cubic structure.^{8,9)} In this paper, we are interested in the mechanism of this peculiar quadrupole ordering.

For the investigation of multipole ordering in Pr compounds, one may think that it is enough to employ an LS coupling scheme since, in general, $4f$ electrons of Pr³⁺ are considered to be almost localized. However, for PrPb₃, the situation does not seem to be so simple. Before the confirmation of the modulated ordering, the possibility of the antiferro quadrupole ordering has been discussed.^{10,11)} Then, the sinusoidal quadrupole ordering has been observed,^{8,9)} but it seems to be difficult to explain it on the basis of a localized picture. Furthermore, in PrPb₃, the Fermi surfaces have been clearly observed in a de Haas-van Alphen (dHvA) experiment,¹²⁾ suggesting that it is necessary to consider the quadrupole ordering from an itinerant picture. However, it seems to be a difficult task to treat multipole ordering from a microscopic viewpoint in f^2 -electron systems. In fact, the mechanism of the modulated antiferro quadrupole ordering in PrPb₃ has not been clarified yet, although more than ten years has passed

since the discovery of the peculiar quadrupole ordering.

For the explanation of multipole ordering concerning multiple f electrons, it seems to be necessary to consider alternative theoretical research complementary to the LS coupling scheme. Thus, we believe that it is meaningful to develop a microscopic theory for multipole ordering from an itinerant picture on the basis of a j - j coupling scheme.¹³⁻¹⁵⁾ In fact, recently, several groups have advanced the theoretical investigation on the multipole ordering in f -electron systems from the microscopic viewpoint by performing first-principles calculations.¹⁶⁻²²⁾ For the multipole order in CeB₆, in which theoretical research based on the LS coupling scheme has been carried out for a long time, but recently, analysis from the itinerant picture has been performed.²³⁾ For the analysis of multipole ordering on the basis of the j - j coupling scheme, we define the multipole operator as the spin-charge density in the form of a one-body operator.¹³⁻¹⁵⁾ Since the f -electron state with angular momentum $\ell = 3$ contains seven orbitals, it is desirable to adopt a seven-orbital Hamiltonian as a realistic f -electron model, if possible. However, such a seven-orbital model is too complicated to be a prototype to develop the microscopic theory of multipole ordering. We also encounter difficulties in interpreting the calculation results, even though we can perform the calculations in the seven-orbital model.¹⁵⁾

Then, we attempt to effectively reduce the number of relevant orbitals. When we consider the local f -electron states on the basis of the j - j coupling scheme,²⁴⁾ we notice that the Γ_3 ground states are mainly composed of two singlets among Γ_7 and Γ_8 electrons.²⁵⁻³⁰⁾ Note that the double degeneracy originates from the orbital degrees of freedom in Γ_8 electrons. This is consistent with the fact that Γ_3 is included in the direct products of Γ_7 and Γ_8 . Thus, we discuss the Γ_3 quadrupole ordering in f^2 -electron systems on the basis of a Γ_7 - Γ_8 three-orbital Hamiltonian.^{26,30)} We evaluate the multipole susceptibility of the model in a random phase approximation (RPA) and attempt to clarify the mechanism of the emergence of incommensurate quadrupole order from a microscopic viewpoint.

In this paper, we construct the Γ_7 - Γ_8 three-orbital model

for the f^2 -electron system from the itinerant picture. Then, we introduce the effective interactions that stabilize the local Γ_3 ground state for the case of $n = 2$. We perform the RPA calculations for the multipole susceptibilities to discuss the condition for the appearance of quadrupole order. We emphasize that the hybridization between Γ_7 and Γ_8 orbitals is important for the emergence of the Γ_3 quadrupole ordering. We also propose a concept of multipole nesting. Namely, the Fermi surface region with large Γ_8 orbital density is nested on the area with a significant Γ_7 component when we shift the positions of Fermi surfaces by the ordering vector. This is consistent with the fact that local Γ_3 doublets are mainly composed of two singlets between Γ_7 and Γ_8 orbitals. Finally, we discuss the possible relevance of the present results to the incommensurate quadrupole ordering observed in PrPb₃ with some comments on future problems.

The paper is organized as follows. In Sect. 2, the model Hamiltonian with effective interactions among f electrons is introduced. After explaining the multipole operators, we provide the formulation to evaluate multipole susceptibilities in the RPA. In Sect. 3, our calculation results on the multipole susceptibilities are shown. We clarify the key quantity, Γ_7 - Γ_8 hybridization, for the emergence of the quadrupole ordering. We attempt to unveil the microscopic mechanism of incommensurate quadrupole ordering by focusing on the Fermi surface nesting property as well as the orbital density distribution on the Fermi surfaces. In Sect. 4, we provide several comments on the quadrupole ordering in the present scenario in comparison with the experimental results observed for PrPb₃. Finally, we summarize this paper. Throughout this paper, $\hbar = k_B = 1$.

2. Model and Formulation

2.1 Model Hamiltonian

To consider the multipole ordering from a microscopic viewpoint on the basis of the itinerant picture, we set the model Hamiltonian as

$$H = H_{\text{kin}} + H_{\text{loc}}, \quad (1)$$

where H_{kin} and H_{loc} denote the kinetic and local terms for f electrons, respectively.

First let us discuss in detail how to construct the local term H_{loc} . To consider the electronic properties of f -electron compounds, the best way is to treat the seven-orbital model, including Coulomb interactions, spin-orbit coupling, and crystalline electric field (CEF) potentials. For instance, the Kondo phenomena have been discussed in detail on the basis of the seven-orbital Anderson model hybridized with several conduction bands. Then, two-channel Kondo effects was found not only in the Pr ion but also in Nd and other rare-earth systems in an unbiased manner.^{31,32)}

Concerning the multipole ordering, the seven-orbital Hubbard model has also been analyzed with the use of the RPA for the evaluation of multipole susceptibility. Such calculations have actually been performed,¹⁵⁾ but it was difficult to clarify the mechanism of the multipole ordering from a microscopic viewpoint, mainly due to the complexity originating from the large number of orbitals. Thus, it is desirable to reduce the number of relevant orbitals to obtain the effective Hamiltonian for the purpose of grasping the essential point concerning the appearance of multipole ordering.

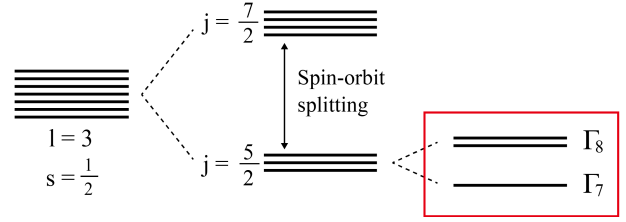


Fig. 1. (Color online) Level splitting of f electron states due to spin-orbit coupling, leading to $j = 7/2$ octet and $j = 5/2$ sextet, where j is the total angular momentum. The sextet of $j = 5/2$ is further split into a Γ_7 doublet and Γ_8 quartet under the cubic CEF potentials. Note that for simplicity, we suppress the Kramers degeneracy in this figure. The effective model is constructed with the use of Γ_7 and Γ_8 bases.

A basic strategy to construct such an effective model is to exploit a j - j coupling scheme.²⁴⁾ As schematically shown in Fig. 1, we first include the effect of spin-orbit coupling in the one- f -electron state characterized by the orbital $\ell = 3$ and spin $s = 1/2$, leading to an octet with a total angular momentum $j = 7/2$ and a sextet with $j = 5/2$. Since the energy of the sextet is lower than that of the octet, we consider the states of the $j = 5/2$ sextet to construct the effective model for rare-earth and actinide compounds for $n \leq 6$. We accommodate f electrons in the level scheme of the one- f -electron states and include the effect of Coulomb interactions among them.

Since we consider the cubic system in this paper, it is convenient to use the cubic irreducible representations. As shown in Fig. 1, under the cubic CEF potentials, the $j = 5/2$ sextet is further split into a Γ_7 doublet and Γ_8 quartet. To distinguish the states in the Γ_8 quartet and Γ_7 doublet, we introduce three pseudo-orbitals τ ($=a, b,$ and c), while pseudospin σ ($=\uparrow$ and \downarrow) is introduced to distinguish the Kramers degeneracy. For the description of the model Hamiltonian, it is useful to define the second-quantized operator $f_{i\tau\sigma}$ with pseudospin σ and pseudo-orbital τ at site i , expressed as

$$f_{i\tau\sigma} = \sum_{\mu} A_{\tau\sigma,\mu} a_{i\mu}, \quad (2)$$

where $a_{i\mu}$ denotes the annihilation operator of an f electron in the $j = 5/2$ sextet with the z -component μ at site i and A indicates the coefficient connecting f and a operators. For Γ_{8a} and Γ_{8b} electrons, f operators are explicitly given by

$$\begin{aligned} f_{ia\uparrow} &= \sqrt{\frac{5}{6}} a_{i-5/2} + \sqrt{\frac{1}{6}} a_{i3/2}, \\ f_{ia\downarrow} &= \sqrt{\frac{5}{6}} a_{i5/2} + \sqrt{\frac{1}{6}} a_{i-3/2}, \end{aligned} \quad (3)$$

and

$$\begin{aligned} f_{ib\uparrow} &= a_{i-1/2}, \\ f_{ib\downarrow} &= a_{i1/2}, \end{aligned} \quad (4)$$

respectively.

For an Γ_7 electron ($\tau = c$), we obtain

$$\begin{aligned} f_{ic\uparrow} &= \sqrt{\frac{1}{6}} a_{i-5/2} - \sqrt{\frac{5}{6}} a_{i3/2}, \\ f_{ic\downarrow} &= \sqrt{\frac{1}{6}} a_{i5/2} - \sqrt{\frac{5}{6}} a_{i-3/2}. \end{aligned} \quad (5)$$

For the standard time-reversal operator $\mathcal{K} = -i\sigma_y K$, where K denotes an operator taking the complex conjugate, we can easily show the relation $\mathcal{K}f_{i\tau\sigma} = \sigma f_{i\tau-\sigma}$, which is the same definition for a real spin.²⁴⁾

Now we consider the local term, which should be composed of the CEF potential and Coulomb interaction terms. However, we include only the latter term in this paper for the reason which we will explain later. The Coulomb interaction term is given in the second-quantized form as

$$H_{\text{loc}} = \sum_{i,1\sim 4} I_{12,34} f_{i1}^\dagger f_{i2}^\dagger f_{i3} f_{i4}, \quad (6)$$

where I indicates the Coulomb interactions and we use shorthand notation such as $1 = \{\tau_1, \sigma_1\}$. Hereafter we use this notation when there is no possibility of confusion.

Concerning the matrix elements of I , there are several methods to evaluate these values. A straightforward way to obtain I is to estimate the Coulomb integrals with the use of f -electron wavefunctions in the limit of large spin-orbit coupling λ .²⁴⁾ This has the merit that we can obtain all the matrix elements analytically, while we encounter a serious problem that a local Γ_3 doublet cannot be stabilized in the limit of infinite λ . To reproduce the local Γ_3 state correctly, it is necessary to consider the effective interaction, including the effect of the sixth-order CEF potentials, expressed by the terms of B_6^0 .³³⁾ A simple way to include the effect of B_6^0 is to perform the perturbation expansion in terms of $1/\lambda$ to take into account the effect of the $j = 7/2$ octet in which the B_6^0 terms are correctly included.³⁴⁾ Another method is to include the effect of B_6^0 through the two-body potential for the $j = 5/2$ sextet.³²⁾ Finally, it is also possible to more systematically obtain the effective interactions to reproduce the low-energy spectrum of the seven-orbital model by maximizing the overlap integrals between the states of the seven-orbital model and those of the three-orbital model.²⁸⁾

In this paper, basically we follow the last method, but we do not pay special attention to the reproduction of the low-energy spectrum of the seven-orbital model. Rather, we simply consider the situation in which the local Γ_3 ground state is stabilized since we are more interested in the mechanism of the Γ_3 quadrupole order. An outline of how to determine the effective interaction is as follows. When we consider local f^2 states in the present three-orbital model, there are 15 eigenstates in total, originating from a nonet ($J = 4$), quintet ($J = 2$), and singlet ($J = 0$),²⁴⁾ where J denotes the total angular momentum of the f^2 multiplet when we suppress the CEF potentials. Note that the nonet of $J = 4$ is the ground-state multiplet due to Hund's rules. When we include the cubic CEF potentials, the nonet of $J = 4$ is further split into four groups: a Γ_1 singlet, Γ_3 doublet, Γ_4 triplet, and Γ_5 triplet. Under the cubic CEF potentials, the quintet of $J = 2$ is split into a Γ_3 doublet and Γ_5 triplet. Namely, the 15 f^2 states are classified into two Γ_1 singlets, two Γ_3 doublets, one Γ_4 triplet, and two Γ_5 triplets. Since the states belonging to the same symmetry are mixed, in general, the interaction term is expressed as

$$H_{\text{int}} = \sum_{i,\Gamma,\gamma,p,p'} V_{pp'}^\Gamma |f_i^2, \Gamma_\gamma^{(p)}\rangle \langle f_i^2, \Gamma_\gamma^{(p')}|, \quad (7)$$

where $V_{pp'}^\Gamma$ indicates the effective interaction, $|f_i^2, \Gamma_\gamma^{(p)}\rangle$ de-

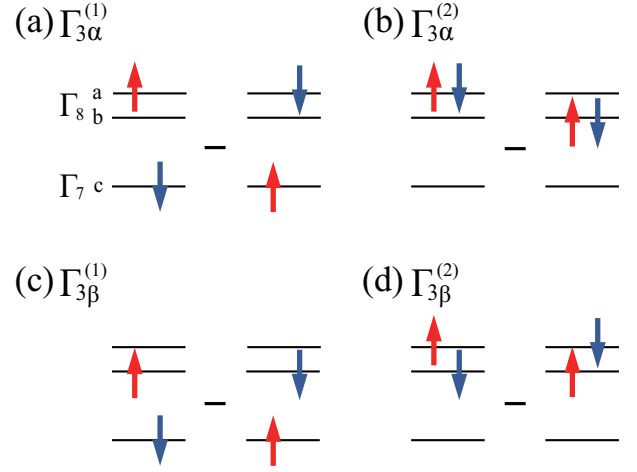


Fig. 2. (Color online) Local Γ_3 states composed of two f electrons. (a) $|f_i^2, \Gamma_{3\alpha}^{(1)}\rangle$, (b) $|f_i^2, \Gamma_{3\alpha}^{(2)}\rangle$, (c) $|f_i^2, \Gamma_{3\beta}^{(1)}\rangle$, and (d) $|f_i^2, \Gamma_{3\beta}^{(2)}\rangle$.

notes the f^2 state at site i , Γ and γ characterize the irreducible representation, and p ($= 1$ and 2) denotes the index used to distinguish the same irreducible representation. Note also that $V_{pp'}^\Gamma$ does not depend on γ .

Let us exhibit all the f^2 states in the following. First, for the Γ_1 singlet states, we obtain

$$|f_i^2, \Gamma_1^{(1)}\rangle = \sqrt{\frac{1}{6}} (f_{ia\uparrow}^\dagger f_{ia\downarrow}^\dagger + f_{ib\uparrow}^\dagger f_{ib\downarrow}^\dagger - 2f_{ic\uparrow}^\dagger f_{ic\downarrow}^\dagger) |0\rangle, \quad (8)$$

$$|f_i^2, \Gamma_1^{(2)}\rangle = \sqrt{\frac{1}{3}} (f_{ia\uparrow}^\dagger f_{ia\downarrow}^\dagger + f_{ib\uparrow}^\dagger f_{ib\downarrow}^\dagger + f_{ic\uparrow}^\dagger f_{ic\downarrow}^\dagger) |0\rangle,$$

where $|0\rangle$ denotes a vacuum.

For the Γ_3 doublet states, we introduce $\gamma = \alpha$ and β to distinguish the doublet. For $\Gamma_{3\alpha}$ and $\Gamma_{3\beta}$, we obtain

$$|f_i^2, \Gamma_{3\alpha}^{(1)}\rangle = \sqrt{\frac{1}{2}} (f_{ic\downarrow}^\dagger f_{ia\uparrow}^\dagger - f_{ic\uparrow}^\dagger f_{ia\downarrow}^\dagger) |0\rangle, \quad (9)$$

$$|f_i^2, \Gamma_{3\alpha}^{(2)}\rangle = \sqrt{\frac{1}{2}} (f_{ia\uparrow}^\dagger f_{ia\downarrow}^\dagger - f_{ib\uparrow}^\dagger f_{ib\downarrow}^\dagger) |0\rangle,$$

and

$$|f_i^2, \Gamma_{3\beta}^{(1)}\rangle = \sqrt{\frac{1}{2}} (f_{ib\uparrow}^\dagger f_{ic\downarrow}^\dagger - f_{ib\downarrow}^\dagger f_{ic\uparrow}^\dagger) |0\rangle, \quad (10)$$

$$|f_i^2, \Gamma_{3\beta}^{(2)}\rangle = \sqrt{\frac{1}{2}} (f_{ia\uparrow}^\dagger f_{ib\downarrow}^\dagger - f_{ia\downarrow}^\dagger f_{ib\uparrow}^\dagger) |0\rangle,$$

respectively. As schematically shown in Fig. 2, $\Gamma_{3\alpha}^{(1)}$ and $\Gamma_{3\beta}^{(1)}$ are given by the singlets between Γ_7 and Γ_8 orbitals, while $\Gamma_{3\alpha}^{(2)}$ and $\Gamma_{3\beta}^{(2)}$ denote the singlets in Γ_8 orbitals. Namely, the indexes α and β used to distinguish the non-Kramers Γ_3 doublets just correspond to a and b orbitals, respectively. Note that the main components of the Γ_3 states from $J = 4$ ($J = 2$) are $\Gamma_{3\alpha}^{(1)}$ and $\Gamma_{3\beta}^{(1)}$ ($\Gamma_{3\alpha}^{(2)}$ and $\Gamma_{3\beta}^{(2)}$).

For the Γ_4 triplet state, we introduce $\gamma = \xi, \eta$, and ζ to distinguish the triple degeneracy, although it is not necessary

to introduce (p) since only one Γ_4 is found. Then, we obtain

$$\begin{aligned} |f_i^2, \Gamma_{4\xi}\rangle &= \left(-\sqrt{\frac{3}{2}} f_{ib\uparrow}^\dagger f_{ic\uparrow}^\dagger - \frac{1}{2} f_{ic\downarrow}^\dagger f_{ia\downarrow}^\dagger \right) |0\rangle, \\ |f_i^2, \Gamma_{4\eta}\rangle &= \sqrt{\frac{1}{2}} (f_{ic\uparrow}^\dagger f_{ia\downarrow}^\dagger + f_{ic\downarrow}^\dagger f_{ia\uparrow}^\dagger) |0\rangle, \\ |f_i^2, \Gamma_{4\zeta}\rangle &= \left(-\frac{1}{2} f_{ic\uparrow}^\dagger f_{ia\uparrow}^\dagger - \sqrt{\frac{3}{2}} f_{ib\downarrow}^\dagger f_{ic\downarrow}^\dagger \right) |0\rangle. \end{aligned} \quad (11)$$

Finally, for the Γ_5 triplet, we again introduce $\gamma = \xi, \eta$, and ζ to distinguish the triple degeneracy. Since we obtain two Γ_5 , it is necessary to prepare p in this case. Then, we obtain

$$\begin{aligned} |f_i^2, \Gamma_{5\xi}^{(1)}\rangle &= \left(\frac{1}{2} f_{ib\uparrow}^\dagger f_{ic\uparrow}^\dagger + \sqrt{\frac{3}{2}} f_{ic\downarrow}^\dagger f_{ia\downarrow}^\dagger \right) |0\rangle, \\ |f_i^2, \Gamma_{5\eta}^{(1)}\rangle &= \sqrt{\frac{1}{2}} (f_{ib\uparrow}^\dagger f_{ic\downarrow}^\dagger + f_{ib\downarrow}^\dagger f_{ic\uparrow}^\dagger) |0\rangle, \\ |f_i^2, \Gamma_{5\zeta}^{(1)}\rangle &= \left(\sqrt{\frac{3}{2}} f_{ic\uparrow}^\dagger f_{ia\uparrow}^\dagger - \frac{1}{2} f_{ib\downarrow}^\dagger f_{ic\downarrow}^\dagger \right) |0\rangle, \end{aligned} \quad (12)$$

and

$$\begin{aligned} |f_i^2, \Gamma_{5\xi}^{(2)}\rangle &= f_{ia\uparrow}^\dagger f_{ib\uparrow}^\dagger |0\rangle, \\ |f_i^2, \Gamma_{5\eta}^{(2)}\rangle &= \sqrt{\frac{1}{2}} (f_{ia\uparrow}^\dagger f_{ib\downarrow}^\dagger + f_{ia\downarrow}^\dagger f_{ib\uparrow}^\dagger) |0\rangle, \\ |f_i^2, \Gamma_{5\zeta}^{(2)}\rangle &= f_{ia\downarrow}^\dagger f_{ib\downarrow}^\dagger |0\rangle. \end{aligned} \quad (13)$$

In the present form of the effective interactions, it is necessary to set 10 parameters for $V_{pp'}^\Gamma$.²⁸⁾ Namely, there are seven diagonal parameters, $V_{11}^{\Gamma_1}, V_{22}^{\Gamma_1}, V_{11}^{\Gamma_3}, V_{22}^{\Gamma_3}, V_{11}^{\Gamma_5}, V_{22}^{\Gamma_5}$, and V^{Γ_4} , while we find three off-diagonal parameters, $V_{12}^{\Gamma_1}, V_{12}^{\Gamma_3}$, and $V_{12}^{\Gamma_5}$. For simplicity, we define $v_1 = V_{12}^{\Gamma_1}, v_3 = V_{12}^{\Gamma_3}$, and $v_5 = V_{12}^{\Gamma_5}$. In this paper, v_3 is a control parameter used to discuss the quadrupole ordering.

Now we explain the reason why we suppress the one-electron CEF potential term H_{CEF} in this paper. Since we use Γ_7 and Γ_8 bases in the present model, the one-electron potential term is given by $H_{\text{CEF}} = b_4 \sum_i (2\rho_{ci} - \rho_{ai} - \rho_{bi})$, where $\rho_{\tau i} = \sum_\sigma f_{i\tau\sigma}^\dagger f_{i\tau\sigma}$, b_4 is the fourth-order CEF parameter.³³⁾ Concerning the experimental finding for the level scheme, we refer to the result for CePb_3 , which is the f^1 compound with the same lattice structure as that of PrPb_3 . For CePb_3 , it has been found that Γ_7 is the ground state and Γ_8 is the excited state,³⁵⁾ indicating that b_4 is positive. Thus, for PrPb_3 , it is recommended to accommodate two f electrons in this level scheme in the j - j coupling scheme. However, this CEF potential term works toward the destruction of the Γ_3 state, which consists of Γ_7 and Γ_8 electrons. We emphasize that our purpose here is to search for the condition for the appearance of Γ_3 quadrupole ordering in the f^2 -electron systems. Thus, we suppress H_{CEF} from the outset in this paper by taking $b_4 = 0$, although we are interested in the effect of the one-electron CEF potential on the Γ_3 quadrupole order.

Now we consider the kinetic term. As emphasized above, in this paper, we discuss the mechanism of the multipole ordering from the itinerant picture in f -electron systems. For this purpose, we include the hopping of f electrons, although we

do not seriously consider the heavy-mass enhancement due to the hybridization between localized and conduction electrons. Then, the kinetic term H_{kin} is expressed as

$$H_{\text{kin}} = \sum_{\mathbf{k}\tau\tau'} \varepsilon_{\mathbf{k}\tau\tau'} f_{\mathbf{k}\tau\sigma}^\dagger f_{\mathbf{k}\tau'\sigma}, \quad (14)$$

where $f_{\mathbf{k}\tau\sigma}^\dagger$ denotes the Fourier transform of $f_{i\tau\sigma}^\dagger$. By considering only the hopping between nearest-neighbor sites, we obtain the one- f -electron energy $\varepsilon_{\mathbf{k}\tau\tau'}$ in a matrix form as

$$\hat{\varepsilon}_{\mathbf{k}} = \begin{pmatrix} t_8 \alpha_{\mathbf{k}} + s_8 \beta_{\mathbf{k}} & -\sqrt{3} s_8 \gamma_{\mathbf{k}} & t_{78} \beta_{\mathbf{k}} \\ -\sqrt{3} s_8 \gamma_{\mathbf{k}} & t_8 \alpha_{\mathbf{k}} - s_8 \beta_{\mathbf{k}} & \sqrt{3} t_{78} \gamma_{\mathbf{k}} \\ t_{78} \beta_{\mathbf{k}} & \sqrt{3} t_{78} \gamma_{\mathbf{k}} & t_7 \alpha_{\mathbf{k}} \end{pmatrix}, \quad (15)$$

where t_i and s_i denote the hopping amplitudes between adjacent Γ_i orbitals, t_{78} indicates the hopping amplitude between adjacent Γ_7 and Γ_8 orbitals, $\alpha_{\mathbf{k}} = \cos k_x + \cos k_y + \cos k_z$, $\beta_{\mathbf{k}} = \cos k_x + \cos k_y - 2 \cos k_z$, and $\gamma_{\mathbf{k}} = \cos k_x - \cos k_y$.

Although four hopping amplitudes (t_7, t_8, s_8 , and t_{78}) are expressed with the use of four Slater-Koster integrals of $(ff\sigma), (ff\pi), (ff\delta)$, and $(ff\phi)$,³⁶⁻³⁸⁾ here we use the four hopping amplitudes as parameters for convenience in this paper. In the following, we set $t_8 = -1.0$ and the energy unit is $|t_8|$. Although we do not explicitly mention the chemical potential term in this paper, the chemical potential μ is appropriately adjusted under the condition of $\langle n \rangle = 2$, where $\langle n \rangle$ denotes the average number of f electrons per site.

Finally, we provide a comment on another effective model. In this paper, we analyze the three-orbital model, which is composed of Γ_7 and Γ_8 orbitals. Since the non-Kramers Γ_3 doublets in the f^2 state are expressed by two local singlets between Γ_7 and Γ_8 orbitals, the Γ_7 - Γ_8 three-orbital model is suitable for the discussion of the multipole ordering in PrPb_3 from a microscopic viewpoint. The Γ_8 two-orbital Hamiltonian is frequently used as the minimal model to discuss the multipole ordering in f -electron systems,^{28,39-45)} but the Γ_3 states composed of a pair of Γ_8 electrons are not the main component of the f^2 states of the Pr ion. Thus, we adopt the Γ_7 - Γ_8 three-orbital model in this paper.

2.2 Multipole susceptibility in the RPA

Now we explain the procedure to calculate the multipole susceptibility in the RPA. First we define the multipole operator in the one-electron-density form by using the cubic tensor operator $T_{\Gamma\gamma}^{(k)}(\mathbf{q})$,¹³⁻¹⁵⁾ where \mathbf{q} is momentum, Γ and γ indicate the irreducible representation for the cubic point group, and k denotes the rank of the multipole. In the second-quantized form, the cubic tensor operators are given by

$$T_{\Gamma\gamma}^{(k)}(\mathbf{q}) = \sum_{\tau, \sigma, \tau', \sigma'} T_{\tau\sigma, \tau'\sigma'}^{(K)} f_{\mathbf{k}\tau\sigma}^\dagger f_{\mathbf{k}+\mathbf{q}\tau'\sigma'}, \quad (16)$$

where we use the shorthand notation $K = \{k, \Gamma\gamma\}$ and the coefficient $T_{\tau\sigma, \tau'\sigma'}^{(K)}$ is given by

$$T_{\tau\sigma, \tau'\sigma'}^{(K)} = \sum_{\mu, \mu', q} G_{\Gamma\gamma, q}^{(k)} O_{q, \mu\mu'}^{(k)} A_{\tau\sigma, \mu} A_{\tau'\sigma', \mu'}. \quad (17)$$

Here q runs between $-k$ and k , $G_{\Gamma\gamma, q}^{(k)}$ is the transformation matrix between spherical and cubic harmonics, and $O_q^{(k)}$ denotes the spherical tensor operator defined in the space of $j = 5/2$. The matrix element of $O_q^{(k)}$ is explicitly calculated

rank	irreducible representations
0	1g
1	4u
2	3g, 5g
3	2u, 4u, 5u
4	1g, 3g, 4g, 5g
5	3u, 4u1, 4u2, 5u

Table I. Irreducible representations for multipoles up to rank 5. Here we use the shorthand notations explained in the main text. Note that at rank 5, two Γ_{4u} triplets appear, which are distinguished as 4u1 and 4u2.

by the Wigner-Eckart theorem as⁴⁶⁾

$$O_{q,\mu\mu'}^{(k)} = \frac{\langle j||O^{(k)}||j\rangle}{\sqrt{2j+1}} \langle j\mu|j\mu'kq\rangle, \quad (18)$$

where $j = 5/2$, $\langle j\mu|j\mu'kq\rangle$ indicates the Clebsch-Gordan coefficient, and $\langle j||O^{(k)}||j\rangle$ is the reduced matrix element for the spherical tensor operator, given by

$$\langle j||O^{(k)}||j\rangle = \frac{1}{2^k} \sqrt{\frac{(2j+k+1)!}{(2j-1)!}}. \quad (19)$$

Note that we define multipole operators from rank 0 to rank 5 in the present model, since the highest rank is given by $2j$. Note also that when we express the multipole moment, we normalize each multipole operator so as to satisfy the orthonormal condition⁴⁷⁾

$$\text{Tr}\{T^{(K)}T^{(K')}\} = \delta_{KK'} = \delta_{kk'}\delta_{\Gamma\Gamma'}\delta_{\gamma\gamma'}, \quad (20)$$

where δ denotes the Kronecker delta.

In Table I, we show the list of the irreducible representations for the possible multipoles up to rank 5. Basically, we express the irreducible representations for multipoles by Bethe notation in this paper, but we use shorthand notations by combining the number of irreducible representations and the parity of time-reversal symmetry, g for gerade and u for ungerade. For instance, for rank 2, we obtain Γ_{3g} and Γ_{5g} , which are simply expressed as “3g” and “5g”, respectively. Concerning the correspondence to Mulliken notation, note that $\Gamma_1 = A_1$, $\Gamma_2 = A_2$, $\Gamma_3 = E$, $\Gamma_4 = T_1$, and $\Gamma_5 = T_2$.

In general, it is necessary to consider the linear combination of multipoles. For instance, multipoles that belong to the same irreducible representation are allowed to be mixed. Thus, we introduce the multipole operator $X_{\mathbf{q}}$ by the linear combination of the cubic tensor operators, given by

$$X_{\mathbf{q}} = \sum_{k,\Gamma\gamma} P_K(\mathbf{q})T_{\Gamma\gamma}^{(k)}(\mathbf{q}), \quad (21)$$

where $P_K(\mathbf{q})$ indicates the coefficient of the multipole operator in rank k and irreducible representation $\Gamma\gamma$.

Next it is necessary to consider a way to determine the coefficient P .¹⁵⁾ For this purpose, we evaluate the multipole susceptibility in the static limit. In the linear response theory, the multipole susceptibility is defined by

$$\chi(\mathbf{q}) = \int_0^{1/T} d\tau \langle X_{\mathbf{q}}(\tau)X_{-\mathbf{q}}(0) \rangle, \quad (22)$$

where T is the temperature, $X_{\mathbf{q}}(\tau) = e^{H\tau}X_{\mathbf{q}}e^{-H\tau}$, and $\langle \dots \rangle$ indicates the thermal average by using H . From

Eqs. (21) and (22), we obtain the multipole susceptibility as

$$\chi(\mathbf{q}) = \sum_{K,K'} P_K \chi_{K,K'}(\mathbf{q}) P_{K'}, \quad (23)$$

where the susceptibility matrix is given by

$$\chi_{K,K'}(\mathbf{q}) = \sum_{1 \sim 4} T_{1,3}^{(K)} \chi_{12,34}(\mathbf{q}) T_{2,4}^{(K')}. \quad (24)$$

Note that we use the shorthand notations. We also note that $T_{i,j}^{(K)*} = T_{j,i}^{(K)}$, where the asterisk denotes the complex conjugate. Then, χ and P should be determined by the maximum eigenvalue χ_{\max} and the corresponding normalized eigenstate of the susceptibility matrix equation, respectively.

To calculate the multipole susceptibility, in this paper, we resort to the RPA on the basis of the perturbation expansion in terms of the Coulomb interactions. In the RPA, the susceptibility is expressed in a compact matrix form as²⁸⁾

$$\hat{\chi} = \hat{\chi}^{(0)}[\hat{1} - \hat{I}\hat{\chi}^{(0)}]^{-1}, \quad (25)$$

where $\hat{1}$ denotes the unit matrix, \hat{I} is the antisymmetrized interaction in the matrix form, and the bare susceptibility $\hat{\chi}^{(0)}$ is given by

$$\chi_{12,34}^{(0)}(\mathbf{q}) = -T \sum_{n,\mathbf{k}} G_{41}^{(0)}(\mathbf{k}, i\omega_n) G_{32}^{(0)}(\mathbf{k} + \mathbf{q}, i\omega_n). \quad (26)$$

Here $\omega_n = \pi T(2n+1)$ is the fermion Matsubara frequency with integer n and $G_{ij}^{(0)}$ is the one-electron Green's function defined from H_{kin} . Note that $G_{ij}^{(0)} = \delta_{\sigma_i, \sigma_j} G_{\tau_i, \tau_j}^{(0)}$.

For actual calculations of $\hat{\chi}^{(0)}$, it is convenient to first diagonalize H_{kin} as

$$H_{\text{kin}} = \sum_{\mathbf{k}\nu\sigma} E_{\mathbf{k}\nu} \tilde{f}_{\mathbf{k}\nu\sigma}^\dagger \tilde{f}_{\mathbf{k}\nu\sigma}, \quad (27)$$

where ν denotes the index used to distinguish the band, $E_{\mathbf{k}\nu}$ is the band energy, and the relation between f and \tilde{f} is expressed as

$$f_{\mathbf{k}\tau\sigma} = \sum_{\nu} U_{\tau,\nu}(\mathbf{k}) \tilde{f}_{\mathbf{k}\nu\sigma}. \quad (28)$$

Then, the bare susceptibility is given as

$$\begin{aligned} \chi_{12,34}^{(0)}(\mathbf{q}) &= \delta_{\sigma_1, \sigma_4} \delta_{\sigma_2, \sigma_3} \sum_{\mathbf{k}, \nu, \nu'} U_{\tau_1, \nu}^*(\mathbf{k}) U_{\tau_4, \nu}(\mathbf{k}) \\ &\times \chi_{\nu, \nu'}(\mathbf{k}, \mathbf{q}) U_{\tau_2, \nu'}^*(\mathbf{k} + \mathbf{q}) U_{\tau_3, \nu'}(\mathbf{k} + \mathbf{q}), \end{aligned} \quad (29)$$

where $\chi_{\nu, \nu'}(\mathbf{k}, \mathbf{q})$ is given by

$$\chi_{\nu, \nu'}(\mathbf{k}, \mathbf{q}) = \frac{f(E_{\mathbf{k}+\mathbf{q}\nu'}) - f(E_{\mathbf{k}\nu})}{E_{\mathbf{k}\nu} - E_{\mathbf{k}+\mathbf{q}\nu'}}, \quad (30)$$

and f is the Fermi distribution function.

For the momentum \mathbf{q} in multipole susceptibility, we divide the first Brillouin zone into $32 \times 32 \times 32$ meshes. Namely, the unit of \mathbf{q} in the present calculation is $\pi/16$. To efficiently perform the \mathbf{k} integration in the bare susceptibility Eq. (29), we exploit the Gauss-Legendre quadrature with due care. First we divide the first Brillouin zone into $16 \times 16 \times 16$ meshes. Then, in each cube, we adopt 8-point Gauss-Legendre quadrature along the k_x , k_y , and k_z directions. In this numerical calculation, we can arrive at low temperatures such as $T/|t_8| = 0.01$.

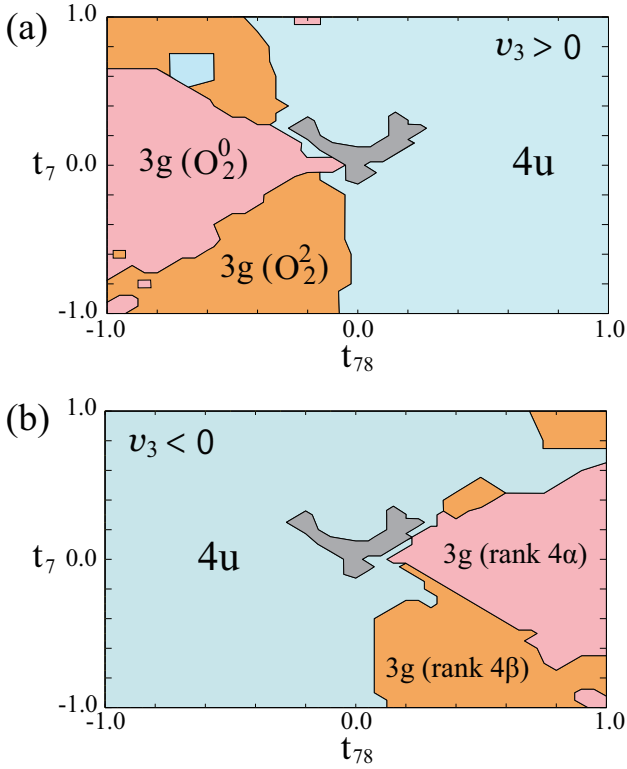


Fig. 3. (Color online) Phase diagrams of the multipole states for (a) $v_3 > 0$ and (b) $v_3 < 0$ on the t_{78} - t_7 plane for $t_8 = -1.0$ and $s_8 = -0.2$. In the gray region, the RPA susceptibilities already diverge even at $v_3 = 0$. Note that 4u and 3g are distinguished by the multipole susceptibility, whereas the kind of 3g multipole state is deduced from the main component in the eigenvector of the multipole susceptibility.

3. Calculation Results

In this section, we show our calculation results for multipole susceptibility. First we discuss the multipole ordered states to reveal the condition for the appearance of quadrupole ordering. Then, we explain that the ordered multipole operators depend on the local ground states stabilized by the effective interactions among f electrons. Furthermore, we show that the Γ_3 quadrupole ordering is induced by both the Γ_7 - Γ_8 hybridization and the Fermi surface structure with a nesting property concerning orbital densities.

For the effective interactions, we set $V_{11}^{\Gamma_1} = 0.3$, $V_{22}^{\Gamma_1} = 0.7$, $V_{11}^{\Gamma_3} = 0.0$, $V_{22}^{\Gamma_3} = 0.5$, $V_{11}^{\Gamma_5} = 0.2$, $V_{22}^{\Gamma_5} = 0.5$, and $V^{\Gamma_4} = 0.1$ for the diagonal parameters. We again emphasize that here we concentrate only on the situation with the local Γ_3 ground state. For the off-diagonal parameters, we simply set $v_1 = v_5 = 0.1$. Then, in this paper, we choose the control parameter as v_3 to always stabilize the local Γ_3 ground state.

3.1 Key role of Γ_7 - Γ_8 hybridization

First we evaluate multipole susceptibility in the RPA and discuss the multipole phase diagram. To determine the ordered multipole state and the corresponding \mathbf{q} , we repeat the calculations of χ_{\max} , the maximum eigenvalue of the RPA susceptibility matrix Eq. (25), while changing the value of v_3 . Note that we consider cases of both $v_3 > 0$ and $v_3 < 0$. In actual calculations, we plot the inverse susceptibility $1/\chi_{\max}$ as a function of v_3 and find the point v_3^S at which $1/\chi_{\max}$ crosses the v_3 axis by extrapolation.

Note that the multipole state among the different irreducible representations is specified by the multipole susceptibility, but the multipoles belonging to the same irreducible representation cannot be distinguished in the present calculations of χ_{\max} . In this paper, the kind of multipole in the same irreducible representation is deduced from the main component in the eigenvector of the corresponding eigenvalue χ_{\max} at $v_3 = \varepsilon v_3^S$, where ε takes a value between 0.9 and 0.98 depending on the hopping parameters.

In Figs. 3(a) and 3(b), we show the phase diagrams for the ordered multipole states for $v_3 > 0$ and $v_3 < 0$, respectively, on the t_{78} - t_7 plane for $t_8 = -1.0$ and $s_8 = -0.2$. The 3g multipole states are classified into O_2^0 , O_2^2 , rank 4α , and rank 4β from the main component in the eigenvector of the corresponding eigenvalue χ_{\max} at $v_3 = \varepsilon v_3^S$. Here we focus on this kind of multipole, while we suppress the information on the ordering vector, which will be separately discussed later. Note that in the present calculations, $v_3 = 0$ does not mean the non-interacting case since there are finite other interactions. In fact, in Figs. 3(a) and 3(b), we find gray regions near $t_{78} = t_7 = 0$, in which the RPA susceptibilities already diverge even at $v_3 = 0$ due to the flat-like Γ_7 band. We are not interested in the gray regions since the magnetic phase is stabilized by an effective interaction other than v_3 .

In Fig. 3(a), as well as for the gray region, we find three regions as one magnetic state and two quadrupole states, O_2^0 and O_2^2 . For $t_{78} < 0$, we mainly obtain the 3g state, but it is found that 85% of this 3g state is rank 2 and 15% is rank 4. Thus, this state is characterized by the 3g quadrupole O_2^0 or O_2^2 . Note that the winner of the competition between O_2^0 and O_2^2 is not determined only by the local conditions, since the local ground states provide the same contribution to O_2^0 and O_2^2 . For $t_{78} \geq 0$, magnetic 4u states appear, which are a mixture of dipoles, octupoles, and dotriacontapoles. We remark that the magnetic multipole state always appears in the present model at $t_{78} = 0$.

On the other hand, as shown in Fig. 3(b), for $v_3 < 0$, two 3g hexadecapole states are stabilized in the region of $t_{78} > 0$. In this case, 95% of the 3g state is rank 4 and 5% is rank 2, indicating that the amounts of ranks 2 and 4 are almost reversed in comparison with the 3g states for $v_3 > 0$. Note that “rank 4α ” and “rank 4β ” in Fig. 3(b) indicate hexadecapoles belonging to the same group as O_2^0 ($\Gamma_{3\alpha}$) and O_2^2 ($\Gamma_{3\beta}$), respectively. For $t_{78} \leq 0$, we again find that 4u magnetic multipole states appear. We suppress the information on the ordering vector \mathbf{Q} in these diagrams, where \mathbf{Q} is defined as the momentum at which the maximum quadrupole susceptibility appears. At this stage, we simply comment that \mathbf{Q} is different even in the same multipole state, depending on the hopping amplitudes.

At $t_{78} = 0$, we find that the magnetic multipole states always appear irrespective of the sign of v_3 . This is consistent with a previous result.³⁰⁾ Namely, the magnetic ground state in the RPA has also been obtained in the three-orbital model including only nearest-neighbor hopping ($ff\sigma$) and the negative Hund’s rule interaction between Γ_7 and Γ_8 electrons. Note that $t_7 = t_{78} = 0$ when we consider only ($ff\sigma$).

Here readers may consider that the above results look strange. Namely, the electric multipole states are not always stabilized, in spite of the choice of the interaction parameters with the local 3g doublet ground state without any dipole moments. In our calculations, we confirm that the stabilized

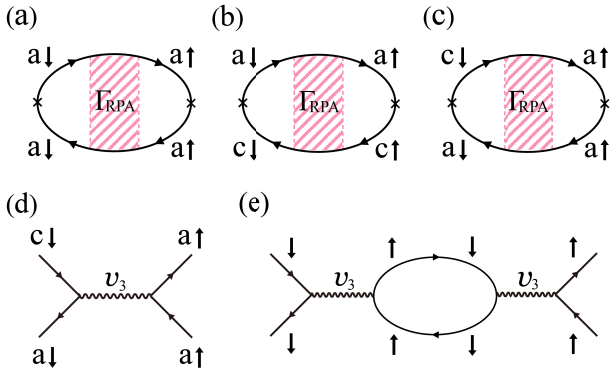


Fig. 4. (Color online) Feynman diagrams for (a) $\chi_{a\downarrow a\uparrow, a\downarrow a\uparrow}$, (b) $\chi_{a\downarrow c\uparrow, c\downarrow a\uparrow}$, and (c) $\chi_{c\downarrow a\uparrow, a\downarrow a\uparrow}$. The hatched rectangle Γ_{RPA} denotes the four-point vertex in the RPA. (d) First- and (e) second-order terms with respect to v_3 of Γ_{RPA} .

multipole state is found to be one of 3g, 4u, and 5u as long as we change v_3 as the control parameter. Note that the 5u octupole appears only in limited parameter regions (not shown here) and the competition between 3g and 4u usually occurs in the present calculations. The ordered multipole moments and corresponding \mathbf{Q} also depend on the hopping parameters and other local parameters. We notice that the multipole phase diagrams for $v_3 > 0$ and $v_3 < 0$ are almost symmetric about the line of $t_{78} = 0$. This tendency is also found when we change hopping parameters t_8 and s_8 . For the stabilization of the 3g quadrupole states, the condition of $t_{78} \neq 0$ is considered to be important.

We find that in the non-interacting case, $\max(\chi_{\max}^{4u}, \chi_{\max}^{5u}) = \max(\chi_{\max}^{1g}, \chi_{\max}^{3g})$, where χ_{\max}^{Γ} indicates the maximum eigenvalue of the susceptibility for the multipole Γ and $\max(A, B)$ indicates the larger value of A and B. The 4u-5u competition as well as the 1g-3g competition in the non-interacting case depends on the hopping amplitudes. With increasing $|v_3|$ for both $v_3 > 0$ and $v_3 < 0$, we observe the enhancement of χ_{\max}^{3g} or χ_{\max}^{4u} .

To understand the competition between magnetic and electric states, we discuss the low-order terms of the RPA susceptibility, which provide significant contributions to the difference between magnetic and electric multipole susceptibilities. It is possible to roughly sketch the phase diagram by the evaluation of such perturbation expansion terms, although the winner of the competition between 3g and 4u is finally determined by the RPA calculations.

We analyze the dependence on σ and τ of the RPA susceptibility by evaluating $\chi_{12,34}(\mathbf{q})$ in Eq. (24) for the RPA susceptibility Eq. (25). After some numerical calculations, we find that the terms shown in Figs. 4(a)-4(c) induce a significant difference between magnetic and electric ($\Gamma_{3\alpha}$) susceptibilities. To estimate the contribution of each Feynman diagram, we consider the first- and second-order terms of Γ_{RPA} in terms of the effective interaction v_3 . When we consider the non-interacting case, the contributions of these Feynman diagrams vanish due to the conservation of pseudospin as long as we take into account only the hopping between nearest-neighbor sites. Namely, the enhancement of such Feynman diagrams strongly depends on the structure of the four-point vertex Γ_{RPA} in the RPA.

In Fig. 4(d), we show the first-order term Γ_{RPA} with respect to v_3 . Here we remark that the local Γ_3 states are composed of two local singlets, as shown in Fig. 2. Note that v_3 is the off-diagonal term between Figs. 2(a) and 2(b) since we consider the $\Gamma_{3\alpha}$ (O_2^0) state. In Fig. 4(d), the Γ_7 state appears just once in the scattering process, leading to the contribution of $G_{ca}G_{aa}^3v_3$ for Fig. 4(a), $G_{ca}^2G_{ac}G_{aa}v_3$ for Fig. 4(b), and $G_{cc}G_{aa}^3v_3$ for Fig. 4(c), where $G_{\tau\tau'}$ denotes the Green's function between τ and τ' orbitals. Next we consider the second-order terms with respect to v_3 , as shown in Fig. 4(e). Since the bubble includes the Green's functions between different pseudospins, the second-order terms simply vanish.

When we repeat the above discussion for higher-order terms with respect to v_3 , we find that Γ_{RPA} never includes the terms of even order of v_3 . Thus, concerning the v_3 dependence, the contributions of Figs. 4(a)-4(c) are expressed by an odd function of v_3 . Concerning the t_{78} dependence, when we expand the Green's function G_{ca} in terms of t_{78} , we notice that G_{ca} is an odd function of t_{78} . Thus, the contributions from Figs. 4(a) and 4(b) are given by an odd function of t_{78} , while that from Fig. 4(c) is considered to be an even function of t_{78} . Then, only for $t_{78} \approx 0$, the contributions of these Feynman diagrams are almost suppressed, even though we change the other hopping parameters t_8 , s_8 , and t_7 . The mechanism can be intuitively understood as follows.

Since the susceptibilities in Figs. 4(a) and 4(b) are considered to be an odd function of t_{78} , they are suppressed for the case of $t_{78} = 0$. Thus, only the Feynman diagram in Fig. 4(c) remains since it includes a term independent of t_{78} . Since other effective interactions such as v_1 and v_5 are found to enhance the magnetic multipole, the enhancement of the electric multipoles shown by the Feynman diagram in Fig. 4(c) is too small to stabilize them, indicating that the susceptibility of the magnetic multipole is always larger than that of the electric multipole at $t_{78} = 0$. Namely, for the stabilization of the 3g quadrupole state, the condition of $t_{78} \neq 0$ is found to be necessary.

From the discussion on the t_{78} and v_3 dependences of the susceptibilities, it is also possible to qualitatively explain the symmetric behavior of the multipole phase diagrams shown in Figs. 3(a) and 3(b) about the line of $t_{78} = 0$. For $t_{78} < 0$ and $v_3 > 0$, the susceptibilities in Figs. 4(a)-4(c) enhance the O_2^0 quadrupole and suppress the 4u multipole, leading to the stabilization of the O_2^0 state. On the other hand, for the case of $v_3 < 0$, the O_2^0 quadrupole should be suppressed since these terms are odd functions of v_3 . Thus, the 4u multipole is stabilized, in sharp contrast to the case of $v_3 > 0$. The appearance of the 3g hexadecapole and 4u multipole in the region of $t_{78} > 0$ can also be understood by the dependence of each term on t_{78} and v_3 in addition to the form of the matrix elements of hexadecapole moments.

3.2 Fermi surface structure and multipole nesting

In this subsection, we discuss the ordering vector \mathbf{Q} of the quadrupole susceptibility when the 3g state is stabilized. Here we point out an important result. As shown in Fig. 5, \mathbf{Q} of the RPA susceptibility is the same as that of the non-interacting susceptibility if the quadrupole state is stabilized. Note that we do not mention the comparison between 3g and 4u multipole states. In the following, we explain this claim in detail.

In Fig. 5, we show Eq. (24) for the RPA susceptibility

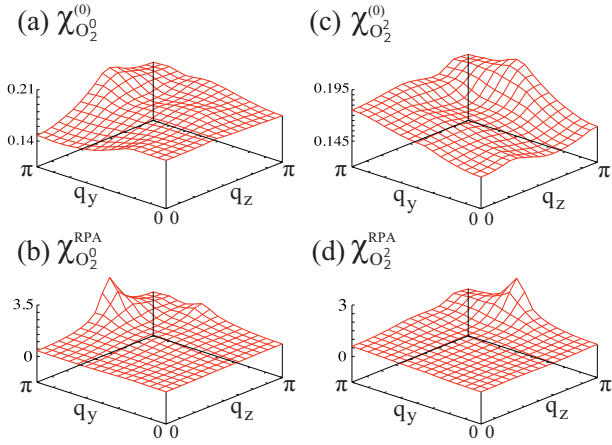


Fig. 5. (Color online) (a) O_2^0 bare susceptibility, (b) O_2^0 RPA susceptibility, (c) O_2^0 bare susceptibility, and (d) O_2^0 RPA susceptibility on the q_y - q_z plane with $q_x = \pi$ for $t_8 = -1.0$, $s_8 = -0.2$, $t_7 = 0.4$, and $t_{78} = -1.0$. In the RPA calculation, the O_2^0 quadrupole state is found to be stabilized for these parameters. To depict (b) and (d), we set $v_3 = 4.0$.

Eq. (25) and the bare susceptibility Eq. (26) with $K = K' = \{2, 3g\alpha\}$. In Figs. 5(a) and 5(b), we show the O_2^0 bare and RPA susceptibilities, respectively, on the q_y - q_z plane with $q_x = \pi$ for $t_8 = -1.0$, $s_8 = -0.2$, $t_7 = 0.4$, and $t_{78} = -1.0$. For these parameters, we obtain the O_2^0 quadrupole state and $\mathbf{Q} = (\pi, \pi, 5\pi/8)$ in the present RPA calculation. In actual calculations, we find that $1/\chi_{\text{max}}$ becomes zero at $v_3^0 = 4.3$. Then, we depict Fig. 5(b) for $v_3 = 4.0$. We emphasize that the peak position of the bare susceptibility in Fig. 5(a) is the same as $\mathbf{Q} = (\pi, \pi, 5\pi/8)$.

In Figs. 5(c) and 5(d), we show the O_2^0 bare and RPA susceptibilities, respectively, for the same parameters as in Figs. 5(a) and 5(b). Namely, these are the results in the O_2^0 quadrupole state. The peak position is found to be $\mathbf{Q} = (\pi, 5\pi/8, \pi)$ for both the bare and RPA susceptibilities. Since the O_2^0 quadrupole ordered state is stabilized, the magnitude of the RPA susceptibility in Fig. 5(d) is smaller than that in Fig. 5(b). It is stressed that the magnitude of the bare susceptibility in Fig. 5(c) is also smaller than that in Fig. 5(a). We notice that this tendency is always observed as long as we consider the quadrupole ordered state in the present research. Namely, it is possible to deduce the kind of quadrupole and the ordering vector \mathbf{Q} in the non-interacting case.

From the analysis of the bare and RPA susceptibilities in the quadrupole state, we notice that the incommensurability of the quadrupole ordering is determined by the Fermi surface structure in the non-interacting case, at least in the RPA. Concerning the effect beyond the RPA, we provide a comment later. Then, hereafter we concentrate on the relation between the Fermi surface structure and the bare susceptibility.

In Fig. 6, we depict the Fermi surfaces for $t_8 = -1.0$, $s_8 = -0.2$, $t_7 = 0.4$, and $t_{78} = -1.0$. The electron Fermi surface in Fig. 6(a) is depicted at the center of the Γ point and is mainly composed of Γ_8 electrons. On the other hand, in Fig. 6(b), we show the hole Fermi surface at the center of the R point, which is composed of Γ_7 electrons. Our Fermi surface structure is similar to the result of the band-structure calculations,¹²⁾ except for the small-size Fermi surface, which is not observed for the present parameters. When we evaluate

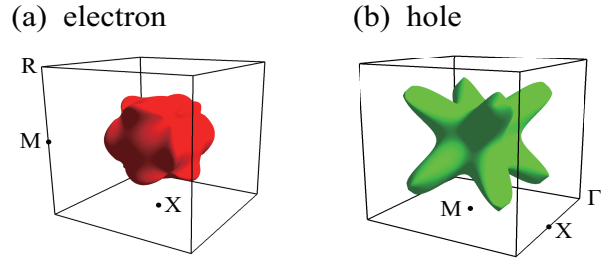


Fig. 6. (Color online) (a) Electron Fermi surface at the center of the Γ point and (b) hole Fermi surface at the center of the R point in the present model for $t_8 = -1.0$, $s_8 = -0.2$, $t_7 = 0.4$, and $t_{78} = -1.0$.

n_7 and n_8 , which are the average electron numbers in the Γ_7 and Γ_8 orbitals per ion, respectively, we obtain $n_7 = 0.79$ and $n_8 = 1.21$ in the present case. These values seem to be consistent with those expected from the local Γ_3 singlets, although there are deviations from $n_7 = n_8 = 1$ due to the difference in the itinerant properties of Γ_7 and Γ_8 electrons.

When we recall the susceptibility of the one-band model, \mathbf{Q} is basically determined from the nesting condition of the Fermi surface. We imagine that the nesting is still important for the determination of \mathbf{Q} of multipole susceptibility in the multiband systems, but it is difficult to conclude the importance of the nesting only from Fig. 6. Thus, we analyze the bare susceptibility in more detail.

For this purpose, we perform the multipole decomposition of the bare susceptibility as in the case of Eq. (24). After some algebraic calculations, we obtain

$$\chi_{K,K'}^{(0)}(\mathbf{q}) = \sum_{\mathbf{k}} \chi_{K,K'}^{(0)}(\mathbf{k}, \mathbf{q}), \quad (31)$$

where $\chi_{K,K'}^{(0)}(\mathbf{k}, \mathbf{q})$ is given by

$$\begin{aligned} \chi_{K,K'}^{(0)}(\mathbf{k}, \mathbf{q}) &= \sum_{\nu\sigma, \nu'\sigma'} L_{\nu\sigma, \nu'\sigma'}^{(K)}(\mathbf{k}, \mathbf{q}) L_{\nu\sigma, \nu'\sigma'}^{(K')*}(\mathbf{k}, \mathbf{q}) \\ &\times \chi_{\nu, \nu'}(\mathbf{k}, \mathbf{q}), \end{aligned} \quad (32)$$

and L is defined as

$$L_{\nu\sigma, \nu'\sigma'}^{(K)}(\mathbf{k}, \mathbf{q}) = \sum_{\tau\tau'} T_{\tau\sigma, \tau'\sigma'}^{(K)} U_{\tau, \nu}^*(\mathbf{k}) U_{\tau', \nu'}(\mathbf{k} + \mathbf{q}). \quad (33)$$

In Fig. 7, we show the results for $t_8 = -1.0$, $s_8 = -0.2$, $t_7 = 0.4$, and $t_{78} = -1.0$. In this case, we have already found that $\mathbf{Q} = (\pi, \pi, 5\pi/8)$ in the O_2^0 susceptibility. Then, we focus on the \mathbf{k} dependence of $\chi_{K,K'}^{(0)}(\mathbf{k}, \mathbf{Q})$ in Eq. (31) for $K = K' = \{2, 3g\alpha\}$. Since it is difficult to depict all the results in the first Brillouin zone, we exhibit $\chi_{K,K'}^{(0)}(\mathbf{k}, \mathbf{Q})$ on the k_x - k_y plane for $k_z = 3\pi/10$ in Fig. 7(a). Note that the value of k_z is chosen for convenience. The spot-like bright regions denote large contributions to the susceptibility, but only from this result, we cannot understand the reason why such regions appear. Then, we show the orbital densities on the curves defined by $E_{\mathbf{k}\nu} = \mu$ and $E_{\mathbf{k}+\mathbf{Q}\nu'} = \mu$ in Figs. 7(b) and 7(c), respectively. We clearly observe that the $\Gamma_{8\alpha}$ and Γ_7 densities become significantly large on the curves defined by $E_{\mathbf{k}\nu} = \mu$ and $E_{\mathbf{k}+\mathbf{Q}\nu'} = \mu$, respectively.

In Fig. 7(d), we consider the nesting between the two curves $E_{\mathbf{k}\nu} = \mu$ and $E_{\mathbf{k}+\mathbf{Q}\nu'} = \mu$ with significant orbital densities. Then, we notice the existence of segments on the

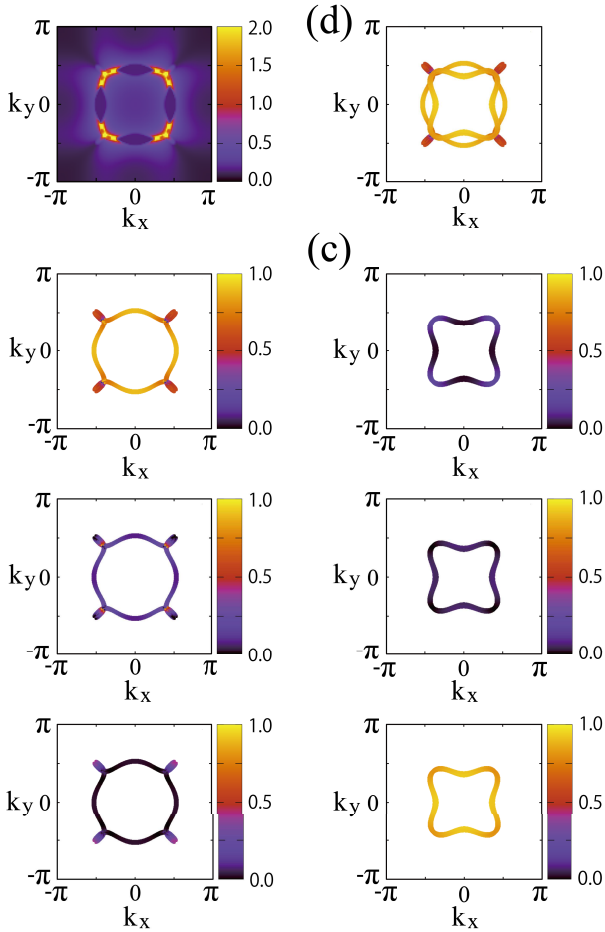


Fig. 7. (Color online) (a) Color plot of $\chi_{K,K'}^{(0)}(\mathbf{k}, \mathbf{Q})$ for $K = K' = \{2, 3g\alpha\}$ on the k_x - k_y plane for $k_z = 3\pi/10$ with $\mathbf{Q} = (\pi, \pi, 5\pi/8)$. (b) Orbital densities on the curve defined by $E_{k\nu} = \mu$. (c) Orbital densities on the curve defined by $E_{k+Q\nu'} = \mu$. (d) Nesting between Γ_{8a} density on the curve of $E_{k\nu} = \mu$ and Γ_7 density on that of $E_{k+Q\nu'} = \mu$.

curves that satisfy the condition of $E_{k\nu} = E_{k+Q\nu'}$, leading to the same positions as the spot-like bright regions in Fig. 7(a). We emphasize the importance of the nesting between the curve of $E_{k\nu} = \mu$ with large Γ_{8a} density and that of $E_{k+Q\nu'} = \mu$ with large Γ_7 density. Namely, for the stabilization of the O_2^0 quadrupole order, it is necessary to obtain the nesting between the Fermi surfaces with Γ_{8a} and Γ_7 densities. Thus, we call it *multipole nesting* in this paper.

For different hopping parameters, the O_2^2 quadrupole state is found in Fig. 3(a). We can depict figures similar to Fig. 7, but here we only explain the difference from Fig. 7 without showing the figures. In the O_2^2 quadrupole state, we observe the multipole nesting between Γ_{8b} and Γ_7 orbital densities. In addition, we also find multipole nesting between Γ_{8a} and Γ_{8b} orbital densities in this case. As shown in Eq. (10), the local $\Gamma_{3\beta}$ doublet is composed of a pair of singlets, but after some algebraic calculations, the singlet between Γ_{8b} and Γ_7 orbitals is found to be the main component of the local $\Gamma_{3\beta}$ doublet. Another singlet between Γ_{8a} and Γ_{8b} gives a minor contribution. This local singlet structure seems to be consistent with the above explanation for the multipole nesting in the O_2^2 quadrupole state.

We provide a comment on the appearance of the 4u magnetic state for $t_{78} \neq 0$. If the multipole nesting properties for

both O_2^0 and O_2^2 are found to be weak, the largest susceptibility among the electric multipoles is the 1g hexadecapole in the non-interacting system. In this situation, the susceptibilities of the quadrupole become smaller than that of the magnetic multipole. Thus, in such a case, the 4u magnetic multipole state is stabilized for $t_{78} \neq 0$.

From the present calculation results, we propose that the O_2^0 (O_2^2) quadrupole ordering is regarded as the quadrupole density wave state composed of Γ_{8a} (Γ_{8b}) and Γ_7 electrons. To stabilize this state, it is necessary to have nesting between the segments on the Fermi surface with large Γ_8 and Γ_7 densities. This is the most important result of this paper.

4. Discussion and Summary

In this paper, we introduced the Γ_7 - Γ_8 model Hamiltonian with the effective interactions that induce the local Γ_3 ground states for $n = 2$. Then, we estimated the multipole susceptibilities in the RPA to reveal the condition for the emergence of Γ_3 quadrupole ordering. We clarified that the Γ_3 quadrupole order can be understood from the concept of multipole nesting, in which the Fermi surface region with large Γ_8 orbital density should be nested on the area with a significant Γ_7 component when we shift the positions of the Fermi surfaces with the ordering vector \mathbf{Q} . This result suggests that the Γ_3 quadrupole ordering can be understood from the combination of the Γ_7 and Γ_8 electrons in the momentum space, corresponding to the local Γ_3 doublets composed of two singlets between Γ_7 and Γ_8 orbitals.

In the present work, we proposed that the quadrupole ordering is regarded as the quadrupole density wave state from the itinerant picture. We believe that our scenario works for the understanding of the Γ_3 quadrupole order in PrPb₃.⁸⁾ First we remark that Fermi surfaces have been observed in PrPb₃ in a dHvA experiment.¹²⁾ This fact seems to support the starting point of our present approach from the itinerant picture for f electrons. Note, however, that the band-structure calculations were carried out for LaPb₃,¹²⁾ not for PrPb₃, probably due to the difficulty in the treatment of non-Kramers Γ_3 states from the itinerant picture. Thus, the contribution of f electrons to the Fermi surfaces seems to be unclear, but we simply assume that a $4f$ -electron admixture should appear, more or less, in the Fermi surfaces. We consider that our present model is constructed for such itinerant f electrons through the hybridization with conduction electrons.

Next we emphasize that the incommensurate quadrupole order in PrPb₃ is considered to be the sinusoidal wave state. It is difficult to reproduce such a state from the localized picture. However, in the itinerant picture, as emphasized in this paper, it is possible to regard it as the quadrupole density wave state. Also from this viewpoint, we believe that the present approach works for PrPb₃.

However, there are some problems in the present approach. One is the incommensurability of the quadrupole order. The ordering vector of the peculiar incommensurate quadrupole state has been found to be $\mathbf{Q}_0 = (\pi, \pi \pm \delta, 0)$ and $(\pi \pm \delta, \pi, 0)$ with $\delta = \pi/4$. Unfortunately, in the present calculations including only the nearest-neighbor hopping, we did not reproduce the quadrupole ordering with \mathbf{Q}_0 . When we include the next-nearest-neighbor hopping and further neighbors, it may be possible to obtain the quadrupole ordering with \mathbf{Q}_0 , but in the present paper, we did not make such an effort for the

parameter tuning for the reason below.

Another problem relates to the choice of local interactions. In this paper, to obtain the Γ_3 quadrupole ordering, we restricted ourselves only to the situation in which the local Γ_3 state is stabilized by the effective interactions chosen by hand. We recognize that it is necessary to further investigate the condition for the effective interactions to obtain the Γ_3 quadrupole ordering from the itinerant picture with realistic parameters.

We emphasize that our purpose is to explore a route to the Γ_3 quadrupole order from the itinerant picture. Thus, we did not thoroughly perform the parameter search for the hopping amplitudes and local interactions within the present model. Such effort may be a future task, but it is more desirable to perform the first-principles calculations to estimate the effective hopping amplitudes and local interactions with the use of the Wannier basis functions.¹⁷⁾ In the thus obtained three-orbital model, it is highly recommend to perform the present calculations for the multipole susceptibility in the RPA. We believe that this is the next step in this direction of research, when we attempt to further develop the present theory for the quadrupole ordering in f^2 -electron systems.

Here we briefly discuss the effect of H_{CEF} . Since it destabilizes the local Γ_3 states composed of Γ_7 and Γ_8 singlets, we ignored this term in this paper, but it may be interesting to consider the quantum critical behavior induced by CEF potentials in the Γ_3 quadrupole ordering. It may be interesting to observe unconventional superconductivity induced by quadrupole fluctuations near such a critical point. This is another future issue.

Finally, we provide a brief comment on the determination of \mathbf{Q} from the interaction viewpoint. We evaluated the multipole susceptibility in the RPA in the present paper and arrived at the picture of multipole nesting for the microscopic understanding of Γ_3 quadrupole ordering. For the ordering vector \mathbf{Q} , within the RPA, we found that \mathbf{Q} in the RPA susceptibility is the same as that in the bare susceptibility. This statement was found to be valid when we investigated the present model by using other effective interactions. It is difficult to prove it mathematically, but we believe that \mathbf{Q} of the quadrupole ordering is determined in the non-interacting case as long as we consider the quasi-particle picture on the basis of the Fermi liquid theory. In the perturbation expansion, it is possible to discuss the peak of susceptibility including the effect of the vertex corrections beyond the RPA.¹⁷⁾ This point is another future problem.

In summary, we discussed the Γ_3 quadrupole ordering in f^2 -electron systems from the microscopic viewpoint. We emphasized the point that the Γ_3 quadrupole order in f^2 -electron systems can be understood from the multipole nesting, in which the Fermi surface region with large Γ_8 orbital density is nested on the area with a significant Γ_7 component when we shift the positions of the Fermi surfaces with the ordering vector. This is the conceptual finding of the present paper, although we have not perfectly explained the Γ_3 quadrupole order in PrPb_3 . The ordering vector will also be explained within the present scheme, for instance, by evaluating hopping and interaction parameters using first-principles calculations, which is a future task.

Acknowledgments

We are grateful to T. Onimaru for the fruitful discussion on the quadrupole ordering in PrPb_3 . We also thank K. Hattori and K. Kubo for discussions and comments. The computation in this work was partly carried out using the facilities of the Supercomputer Center of the Institute for Solid State Physics, University of Tokyo. This work was supported by JSPS KAKENHI Grant Numbers JP16H04017 and JP17J05394.

- 1) T. Hotta, Rep. Prog. Phys. **69**, 2061 (2006).
- 2) Y. Kuramoto, H. Kusunose, and A. Kiss, J. Phys. Soc. Jpn. **78**, 072001 (2009).
- 3) P. Santini, S. Carretta, G. Amoretti, R. Caciuffo, N. Magnani, and G. H. Lander, Rev. Mod. Phys. **81**, 807 (2009).
- 4) T. Onimaru and H. Kusunose, J. Phys. Soc. Jpn. **85**, 082002 (2016).
- 5) H. Kusunose, J. Phys. Soc. Jpn. **77**, 064710 (2008).
- 6) D. L. Cox, Phys. Rev. Lett. **59**, 1240 (1987).
- 7) D. L. Cox and A. Zawadowski, *Exotic Kondo Effects in Metals* (Taylor & Francis, London, 1999).
- 8) T. Onimaru, T. Sakakibara, N. Aso, H. Yoshizawa, H. S. Suzuki, and T. Takeuchi, Phys. Rev. Lett. **94**, 197201 (2005).
- 9) Y. Sato, H. Morodomi, K. Ienaga, Y. Inagaki, T. Kawae, H. S. Suzuki, and T. Onimaru, J. Phys. Soc. Jpn. **79**, 093708 (2010).
- 10) T. Tayama, T. Sakakibara, K. Kitami, M. Yokoyama, and Z. Kletowski, J. Phys. Soc. Jpn. **70**, 248 (2001).
- 11) T. Onimaru, T. Sakakibara, A. Harita, T. Tayama, D. Aoki, and Y. Ōnuki, J. Phys. Soc. Jpn. **73**, 2377 (2004).
- 12) D. Aoki, Y. Katayama, R. Settai, Y. Inada, Y. Ōnuki, H. Harima, and Z. Kletowski, J. Phys. Soc. Jpn. **66**, 3988 (1997).
- 13) T. Hotta, J. Phys. Soc. Jpn. **76**, 083705 (2007).
- 14) T. Hotta, J. Phys. Soc. Jpn. **77** Suppl. A, 96 (2008).
- 15) T. Hotta, Phys. Res. Int. **2012**, 762798 (2012).
- 16) K. Haule and G. Kotliar, Nat. Phys. **5**, 796 (2009).
- 17) H. Ikeda, M.-T. Suzuki, R. Arita, T. Takimoto, T. Shibauchi, and Y. Matsuda, Nat. Phys. **8**, 528 (2012).
- 18) M.-T. Suzuki and H. Ikeda, Phys. Rev. B **90**, 184407 (2014).
- 19) M.-T. Suzuki, N. Magnani, and P. M. Oppeneer, Phys. Rev. B **82**, 241103(R) (2010).
- 20) M.-T. Suzuki, N. Magnani, and P. M. Oppeneer, Phys. Rev. B **88**, 195146 (2013).
- 21) M.-T. Suzuki, T. Koretsune, M. Ochi, and R. Arita, Phys. Rev. B **95**, 094406 (2017).
- 22) M.-T. Suzuki, H. Ikeda, and P. M. Oppeneer, J. Phys. Soc. Jpn. **87**, 041008 (2018).
- 23) A. Koitzsch, N. Heming, M. Knupfer, B. Büchner, P. Y. Portnichenko, A. V. Dukhnenko, N. Y. Shitsevalova, V. B. Filipov, L. L. Lev, V. N. Strocov, J. Ollivier, and D. S. Inosov, Nat. Commun. **7**, 10876 (2016).
- 24) T. Hotta and K. Ueda, Phys. Rev. B **67**, 104518 (2003).
- 25) S. Yotsuhashi, K. Miyake, and H. Kusunose, J. Phys. Soc. Jpn. **71**, 389 (2002).
- 26) H. Onishi and T. Hotta, J. Phys. Soc. Jpn. **77** Suppl. A, 199 (2008).
- 27) K. Kubo and T. Hotta, Phys. Rev. B **95**, 054425 (2017).
- 28) K. Hattori, T. Nomoto, T. Hotta, and H. Ikeda, J. Phys. Soc. Jpn. **86**, 113702 (2017).
- 29) K. Kubo and T. Hotta, J. Phys.: Conf. Ser. **969**, 012096 (2018).
- 30) K. Kubo, J. Phys. Soc. Jpn. **87**, 073701 (2018).
- 31) T. Hotta, J. Phys. Soc. Jpn. **86**, 083704 (2017).
- 32) T. Hotta, Physica B **536**, 203 (2018).
- 33) M. T. Hutchings, Solid State Phys. **16**, 227 (1964).
- 34) T. Hotta and H. Harima, J. Phys. Soc. Jpn. **75**, 124711 (2006).
- 35) D. Nikl, I. Kouroudis, W. Assmus, B. Lüthi, G. Bruls, and U. Welp, Phys. Rev. B **35**, 6864 (1987).
- 36) J. C. Slater and G. Koster, Phys. Rev. **94**, 1498 (1954).
- 37) R. R. Sharma, Phys. Rev. B **19**, 2813 (1979).
- 38) K. Takegahara, Y. Aoki, and A. Yanase, J. Phys. C **13**, 583 (1980).
- 39) R. Shiina, H. Shiba, and P. Thalmeier, J. Phys. Soc. Jpn. **66**, 1741 (1997).
- 40) R. Shiina, O. Sakai, H. Shiba, and P. Thalmeier, J. Phys. Soc. Jpn. **67**, 941 (1998).

- 41) Y. Kuramoto and H. Kusunose, J. Phys. Soc. Jpn. **69**, 671 (2000).
- 42) H. Kusunose and Y. Kuramoto, J. Phys. Soc. Jpn. **70**, 1751 (2001).
- 43) K. Kubo and T. Hotta, Phys. Rev. B **71**, 140404(R) (2005).
- 44) K. Kubo and T. Hotta, Phys. Rev. B **72**, 144401 (2005).
- 45) R. Yamamura and T. Hotta, Physica B: Condens. Matter **536**, 6 (2018).
- 46) T. Inui, Y. Tanabe, and Y. Onodera, *Group Theory and Its Applications in Physics* (Springer, Berlin, 1996).
- 47) K. Kubo and T. Hotta, J. Phys. Soc. Jpn. **75**, 013702 (2006).